


Multidirectional Gradient Feature With Shape Index for Effective Texture Classification

Xi Chen, Guizhou Normal University, China*

 <https://orcid.org/0000-0002-4206-1958>

Jiangmei Li, Guizhou Normal University, China

Yun Fei Zhang, Guizhou Normal University, China

ABSTRACT

Recently, local gradient microstructure of image textures has become an important field of texture classification, but it is generally to investigate the multiscale local microstructures of image gradient, and rarely consider the multidirectional and multiscale local microstructure of image gradient. The proposed algorithm first extracts the two-order gradient feature of the image from different orthogonal directions and further constructs the multiple shape index of the image, and then calculates the histogram feature vectors of the shape index on different orthogonal directions and scales, and finally connects all histogram feature vectors on different orthogonal directions and scales to obtain the final matching feature vector of the image. To further enhance the discriminant ability of feature vector generated by multidirectional shape index schemes, the weight of each block of images is also considered. Experiments on two texture databases and one palmprint database have fully confirmed the effective of proposed algorithm.

KEYWORDS

Linear Projection Subspace, Multidirectional Gradient, Shape Index, Texture Feature Extraction

1. INTRODUCTION

Computer vision and machine learning are critical for image retrieval (Liao et al., 2018), fault recognition, automatic control, automatic driving, ensemble learning (Liu et al., 2018), block chain, vehicle communications, target detection, and tracking (Akhilesh Mohan Srivastava, 2022; Seddik et al., 2022; Thanh, 2022). Image texture has played an important role in computer vision and machine learning since the 1960s (Julesz, 1962). It has been widely studied and applied in many fields, such as image segmentation (Li et al., 2018), content-based image retrieval (Zheng et al., 2018), target detection and recognition (Marszalek et al., 2007; Oyallon & Mallat, 2015), biometrics recognition (Ding et al., 2016; Vu, 2003; Xi & Zhang, 2011; Zhang et al., 2009; Zhao & Pietikainen, 2007), computer graphics, and image texture synthesis (Gatys et al., 2016).

Typical methods of image texture analysis include statistics-based methods (Chellappa & Chatterjee, 1985; Haralik et al., 1973), filtering-based methods (Bovik et al., 1990; Han & Ma, 2007; Mallat, 1989; Randen & Husy, 1999), invariant texture feature description methods (Alata et

DOI: 10.4018/IJSWIS.312183

*Corresponding Author

This article published as an Open Access article distributed under the terms of the Creative Commons Attribution License (<http://creativecommons.org/licenses/by/4.0/>) which permits unrestricted use, distribution, and production in any medium, provided the author of the original work and original publication source are properly credited.

al., 1998; Cohen et al., 1991; Manian & Vasquez, 1998; Wu, 1995), fractal-based methods (Varma & Garg, 2007; Xi & Zhang, 2014), and deep learning-based methods (Andrearczyk & Whelan, 2016; Bu et al., 2019; Chan et al., 2015). The local binary pattern is a relatively simple and effective image local texture description operator. In the book *Computer Vision Using Local Binary Pattern* by Pietikainen et al. in 2011, the basic theory of local binary pattern (LBP) and various applications in pattern recognition and computer vision are introduced (Ojala et al., 2002). Local binary pattern has been widely studied and applied recently. Many researchers have done effective research on it to improve the performance of local binary patterns. The dominant local binary pattern (DLBP) selects the rotation invariant pattern of higher frequency to construct the feature vector, which reduces the length of the feature vector and maintains the discrimination ability of the feature vector (Liao et al., 2009). Considering that the local binary pattern only considers the symbol characteristics of the local difference in pixels, the complete local binary pattern (CLBP) (Guo et al., 2010) considers the symbol, amplitude, and central pixel information of the local difference at the same time. Rotation invariant texture feature extraction is also a key element of improvement (Mehta & Egiazarian, 2015). El Merabet et al. (2019) obtained the texture information about microstructure and macrostructure by considering four triples corresponding to the vertical and horizontal directions and two diagonal directions. Chakraborty et al. (2018) proposed a center symmetric quadruple pattern (CSQP), which effectively encodes the large neighborhood of the face with the best binary digits in the quadruple space. Some researchers converted the original image into multiple images with the aid of some high-pass and low-pass filters, then calculated the local descriptor of each filtered image, and finally connected it into a single descriptor (Dubey, 2019a). Ding et al. (2016) proposed a new scheme for multidirectional multistage double crossover pattern (MDMLDCPS). Specifically, the MDMLDCPS scheme uses the first derivative of the Gaussian operator to reduce the impact on lighting, and then calculates dual cross patterns (DCP) features on the overall and component levels. Dubey et al. (2016) proposed a local plane transformation scheme to calculate the local plane transformation value of each image pixel from the bit plane binary content of each adjacent pixel. Dubey (2019b) also used the relationship between the central pixel and the encoded directional neighborhood to form the proposed local directional relationship pattern (LDRP). Local directional number (LDN) pattern calculated each local microstructure information using a significant direction index (direction number) and symbols (Rivera et al., 2013). Jin et al. (2004) considered the local shape and texture information rather than the original gray information, so they proposed a local binary pattern (ILBP) with improved robustness to illumination changes. Sucharitha and Senapati (2019) proposed the local direction edge binary pattern (LDEBP) algorithm, which collects information from all possible directions, and then calculated the direction information according to the symbol code size of the local difference from the central pixel to its direction pixel. The local optimal direction pattern encodes the rotation invariance of the local microstructure, which improves the accuracy and time complexity (Chakraborti et al., 2018). Verma and Raman (2017) proposed a local neighborhood difference mode (LNDP) algorithm complementary to the traditional LBP, which converts the relationship of all adjacent pixels in the binary mode. The local binary pattern can also be combined with other algorithms, such as filtering the image with a two-dimensional Gabor filter, and then encoding the filtered result from the local binary pattern (Zhang et al., 2007). It can also reduce the dimensions of histogram feature vectors in a local binary pattern (Chan et al., 2007). Local binary pattern essentially describes the first-order differential information of image pixels, and some researchers have studied the second-order differential properties of the images based on local binary pattern, such as two typical local pattern algorithms based on second-order differential: local differential mode (LDP) (Zhang et al., 2010) and local convex and concave pattern (Alpaslan & Hanbay, 2020; El Merabet & Ruichek, 2018; Xi et al., 2016). In the paper published in 2016, they proposed a local convex-and-concave pattern algorithm to describe the second-order texture features of the image, then El Merabet and Ruichek proposed a similar local convex and concave microstructure pattern (LCvMSP) algorithm in 2018, and then Alpaslan and Hanbay proposed a multi-scale local convex and concave pattern algorithm in 2020,

and encoded the local convex-and-concave features of the texture with “shape index”(SI-LCvMSP). The multiscale local convex and concave pattern algorithm proposed by Alpaslan and Hanbay only considers the two-order gradient of the image at different scales, and does not consider the two-order gradient of the image in different directions. As the gradient of the image has obvious directionality, considering the gradient of the image in different directions and scales simultaneously, more image texture information can be extracted.

Based on the work of Alpaslan and Hanbay (2020), this paper uses a modified shape index to encode two-order gradient of images in different orthogonal directions, and maps the encoded features to the linear discrimination subspace to reduce the length of the feature vector and improve the discrimination ability of the feature vector. The rest of this paper is organized as follows. Section 2 describes the scheme of multidirectional two-order gradient features of an image. Section 3 introduces the basic method for multidirectional shape index, and Section 4 describes the method for producing the texture local microstructure pattern based on the multidirectional shape index. Experimental results verify the proposed texture feature extraction and matching method in Section 5, where a brief description of the database, the comparison and analysis of several related algorithms using the cumulative matching characteristic curve, the comparison of the recognition rate of several related algorithms, and the analysis of the recognition rate after dimension reduction of the eigenvector is included. Section 6 introduces the weighted multidirectional shape index. The last section summarizes the paper.

2. BACKGROUND

The gradient of an image I in a certain direction θ and a certain scale σ is defined by the directional derivative. The specific steps are as follows:

1. The Gaussian function $G(x, y, \sigma)$ is used to smooth the image I , where σ is the scale parameter of the Gaussian function and “*” is the convolution operator:

$$I' = I * G(x, y, \sigma) \quad (1)$$

The Gaussian function is:

$$G(x, y, \sigma) = \frac{1}{2\pi\sigma^2} \exp\left(-\frac{x^2 + y^2}{2\sigma^2}\right) \quad (2)$$

According to the differential property of convolution, the second-order directional derivative in the direction θ of the smoothed image I' is as follows:

$$I_{\theta}^{\sigma} = I * G_{\theta}(x, y, \sigma) \quad (3)$$

where I_θ^σ is the second-order directional derivative of the image I' at direction θ and scale σ . $G_\theta(x, y, \sigma)$ is the second-order directional derivative of the Gaussian function in the direction θ and scale σ , which is defined as follows:

$$G_\theta(x, y, \sigma) = \frac{\partial^2 G}{\partial x^2} \cos^2 \theta + 2 \frac{\partial^2 G}{\partial x \partial y} \sin \theta \cos \theta + \frac{\partial^2 G}{\partial y^2} \sin^2 \theta \quad (4)$$

where:

$$\frac{\partial^2 G}{\partial x^2} = \frac{1}{2\pi\sigma^4} \left(\frac{x^2}{\sigma^2} - 1 \right) e^{-\left(\frac{x^2+y^2}{2\sigma^2}\right)}$$

$$\frac{\partial^2 G}{\partial x \partial y} = \frac{xy}{2\pi\sigma^6} e^{-\left(\frac{x^2+y^2}{2\sigma^2}\right)}$$

and:

$$\frac{\partial^2 G}{\partial y^2} = \frac{1}{2\pi\sigma^4} \left(\frac{y^2}{\sigma^2} - 1 \right) e^{-\left(\frac{x^2+y^2}{2\sigma^2}\right)}$$

Supposing:

$$\frac{\partial^2 G}{\partial x^2} = G_{xx}, \quad \frac{\partial^2 G}{\partial x \partial y} = G_{xy}$$

and:

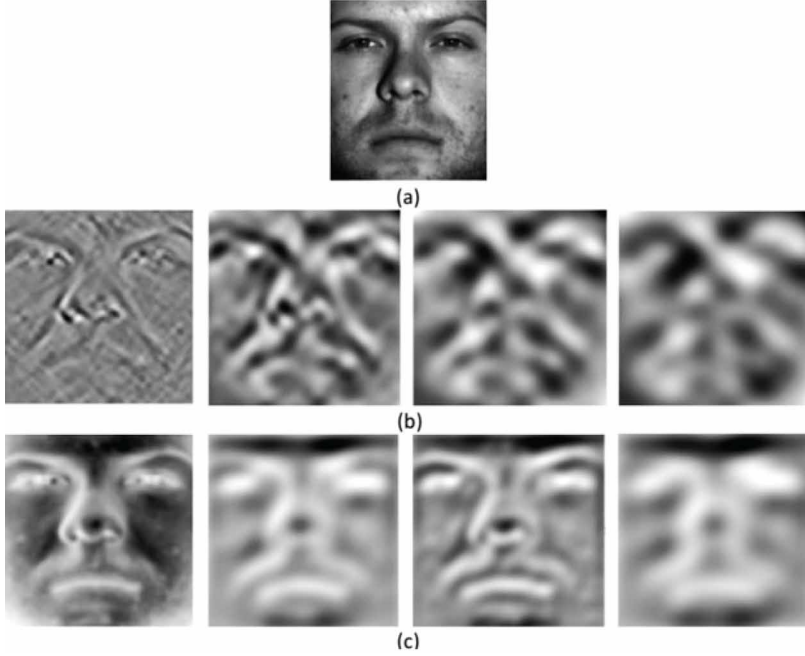
$$G_{xy} = \frac{\partial^2 G}{\partial x \partial y}$$

one gets:

$$G_\theta(x, y, \sigma) = G_{xx} \cos^2 \theta + 2G_{xy} \sin \theta \cos \theta + G_{yy} \sin^2 \theta \quad (5)$$

Figure 1 (a) is a face image; Figure 1 (b) is a gradient image of the face image with different directions and scales; Figure 1(c) is the shape index of the face image with different directions. As can be seen from Figure 1, the two-order gradient information at different directions and scales is clearly different. The larger the scale, the smoother the facial features.

Figure 1. (a) one image from Yale B database; (b) two-order gradient of one image from Yale B database at direction $\theta = 0$ and scale $\sigma = 0.25, 0.5, 1, 2$ (from left to right); (c) two-order gradient of one image from Yale B database at direction $\theta = \frac{\pi}{4}$ and scale $\sigma = 0.25, 0.5, 1, 2$ (from left to right)



3. MULTIDIRECTIONAL GRADIENT FEATURE BASED ON SHAPE INDEX

“Shape index” originates from differential geometry (Koenderink & Van Doorn, 1992). Researchers calculate the “shape index” by means of principal curvature and local second-order differentiation and use it for texture classification (Song et al., 2018). Alpaslan and Hanbay (2020) recently proposed a new and effective method to calculate the “shape index”:

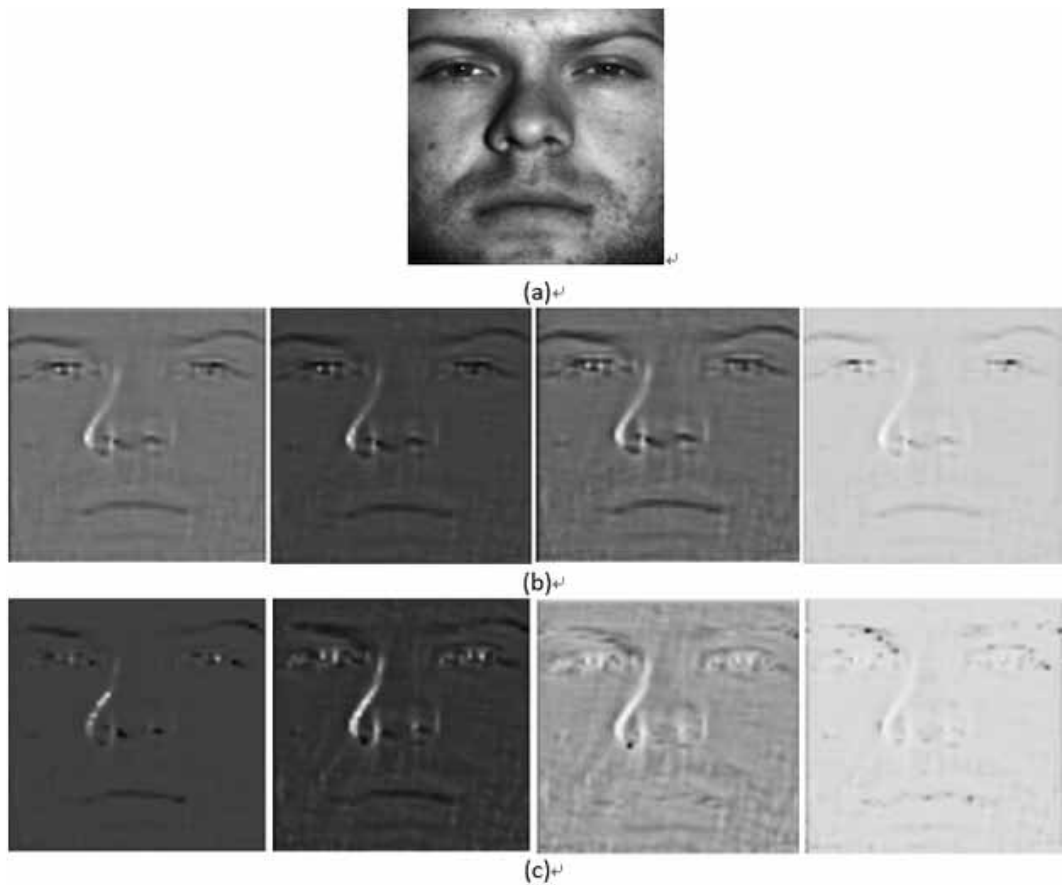
$$S(u, v) = \frac{1}{2} - \frac{1}{\pi} \frac{-I_{xx}(u, v) - I_{yy}(u, v)}{\sqrt{(I_{xx}(u, v) - I_{yy}(u, v))^2 + 4I_{xy}^2(u, v)}} \quad (6)$$

where $I_{xx}(u, v)$, $I_{yy}(u, v)$, and $I_{xy}(u, v)$ represent the second derivative of the texture image at position (u, v) along the X-axis, Y-axis, and the diagonal direction at the first quadrant, respectively. $S(u, v)$ is the “shape index” of the image I at position (u, v) . Because the above calculation for “shape index” only considers the second derivative of the image in the X-axis, Y-axis, and the diagonal direction at the first quadrant, the authors constructed the multidirectional gradient feature on “shape index” as following:

$$S_{\theta}(u, v) = \frac{1}{2} - \frac{1}{\pi} \left(-I_{\theta}^{\sigma}(u, v) - I_{\theta+\pi/2}^{\sigma}(u, v) \right) / \sqrt{\left(I_{\theta}^{\sigma}(u, v) - I_{\theta+\pi/2}^{\sigma}(u, v) \right)^2 + 4 \left(I_{\theta+\pi/4}^{\sigma}(u, v) \right)^2} \quad (7)$$

where $I_{\theta,\sigma}(u,v)$ represents the second derivative of the image I at position (u,v) at direction θ and scale σ . This second derivative can be calculated according to formula (3) and (5). According to formula (7), one can calculate the modified shape index at any point of image I at direction θ and scale σ . Figure 2 shows the modified shape index of one image (b) from the Yale B database.

Figure 2. (a) one image from Yale B database; (b) modified shape index of a face image at scale $\sigma = 0.25$ and direction $\theta = 0, \pi/4, 2 * \pi/4, 3 * \pi/4$ (from left to right); (c) modified shape index of a face image at scale $\sigma = 0.5$ and direction $\theta = 0, \pi/4, 2 * \pi/4, 3 * \pi/4$



4. LOCAL MICROSTRUCTURE OF TEXTURE BASED ON MULTIDIRECTIONAL SHAPE INDEX

After calculating the modified shape index of any point in the image I at direction θ and scale σ according to formula (7), the authors encode the “modified shape index” by local convex and concave pattern. Local convex and concave pattern is an important image texture descriptor proposed by the authors in 2016 (Xi, 2016). Later, other researchers proposed similar methods and performed a more detailed analysis (Alpaslan & Hanbay, 2020; El Merabet & Ruichek, 2018). Since the convex and concave pattern proposed by El Merabet and Ruichek has a more complete mathematical description,

the authors used their model to construct the local convex and concave microstructure pattern based on multidirectional and multiscale shape index (MDSI-LCvMSP). In MDSI-LCvMSP, the local convex and concave microstructure pattern coding of one image at the position (u, v) is as follows:

$$\begin{aligned}
 f_{MDSI-LCvMSP}(u, v) &= \sum_{p=0}^{P-1} \phi(S_p, S(u, v), S_{(p+d) \bmod P}) \\
 &\times 2^{P-1-p} + \phi\left(\frac{1}{P+1} \left(\sum_{p=0}^{P-1} S_p + S(u, v) \right), S(u, v), \lambda\right) \times 2^P \\
 &+ \phi\left(\frac{\sum_{m=1}^M \sum_{n=1}^N S(m, n)}{M \times N}, \bar{S}_c, \bar{\lambda}\right) \times 2^{P+1} - 1
 \end{aligned} \tag{8}$$

where $f_{MDSI-LCvMSP}(u, v)$ represents the MDSI-LCvMSP coding value of the image at position (u, v) , and $S(u, v)$ represents the value of the modified shape index matrix of image I at position (u, v) . S_p represents the p th neighbor of $S(u, v)$. $S_{(p+d) \bmod P}$ represents the $(p+d) \bmod P$ neighbor of $S(u, v)$, P is the total number of neighbors of $S(u, v)$, and d can be set to 1 or 2 or 3 (El Merabet & Ruichek, 2018). λ represents the average value of the modified shape index of the 3x3 adjacent window, and $\bar{\lambda}$ represents the average value of the modified shape index of the entire texture image. M represents the number of rows of the image matrix and N represents the number of columns of the image matrix. $\phi(x, y, z)$ is defined as follows:

$$\phi(x, y, z) = \begin{cases} 1 & \text{if } x \geq y \text{ and } z \geq y \\ 0 & \text{otherwise} \end{cases} \tag{9}$$

The calculation method of MDSI-LCvMSP is introduced through formulas (7), (8), and (9). Next, the authors further introduce our design of MDSI-LCvMSP. This scheme can be summarized as follows:

Step 1: Suppose that an image I is evenly divided into nonoverlapping 4×4 subblocks, which are represented as $I^{(i)}$ ($i = 0, 1, 2, \dots, 15$), respectively.

Step 2: It is assumed that a total of 4 scales $\sigma_0, \sigma_1, \sigma_2, \sigma_3$ and 5 directions $\theta_0, \theta_1, \theta_2, \theta_3, \theta_4$ are used in our scheme. Suppose that the second-order directional derivative of subblock $I^{(i)}$ at direction θ_m and scale σ_n is $I^{(i), \theta_m, \sigma_n}$ ($m = 0, 1, 2, 3, n = 0, 1, 2, 3, 4$) where m denotes the index of scale, n denotes the index of direction, and i denotes the index of subblock.

Step 3: Calculate the second-order directional derivative of each subblock at different directions and scales and the modified shape index matrix of each subblock in light of formula (7).

Step 4: Calculate the texture local microstructure features of the image in light of formula (8). The result is assumed to be $f_{MDSI-LCvMSP}^{I^{(i), \theta_m, \sigma_n}}$ ($i = 0, 1, 2, \dots, 15, \sigma_n = \sigma_0, \sigma_1, \sigma_2, \sigma_3, \theta_m = \theta_0, \theta_1, \theta_2, \theta_3, \theta_4$).

Step 5: Calculate the histogram feature vector of $f_{MDSI-LCvMSP}^{I(i),\theta_m,\sigma_n}$ ($i = 0, 1, 2, \dots, 15$, $\sigma_n = \sigma_0, \sigma_1, \sigma_2, \sigma_3$, $\theta_m = \theta_0, \theta_1, \theta_2, \theta_3, \theta_4$) as $H_{MDSI-LCvMSP}^{I(i),\theta_m,\sigma_n}$. Then, the histogram feature vectors of different subblocks are connected to generate the histogram feature vector of image I :

$$H_{MDSI-LCvMSP}^I = \left[H_{MDSI-LCvMSP}^{I(1)}, H_{MDSI-LCvMSP}^{I(2)}, \dots, H_{MDSI-LCvMSP}^{I(15)} \right] \quad (10)$$

Step 6: Assuming that the feature vectors of MDSI-LCvMSP of two images are $H_{MDSI-LCvMSP}^I$ and $H_{MDSI-LCvMSP}^J$, respectively, the distance between vectors $H_{MDSI-LCvMSP}^I$ and $H_{MDSI-LCvMSP}^J$ is defined as the histogram cross distance:

$$\chi^2 \left(H_{MDSI-LCvMSP}^I, H_{MDSI-LCvMSP}^J \right) = \sum_{i=1}^K \frac{\left(H_{MDSI-LCvMSP}^I(i) - H_{MDSI-LCvMSP}^J(i) \right)^2}{\left(H_{MDSI-LCvMSP}^I(i) + H_{MDSI-LCvMSP}^J(i) + eps \right)} \quad (11)$$

where K is the length of the vector $H_{MDSI-LCvMSP}^I$ or $H_{MDSI-LCvMSP}^J$, and eps is a very small normal number to ensure that $H_{MDSI-LCvMSP}^I(i) + H_{MDSI-LCvMSP}^J(i) + eps$ is not zero.

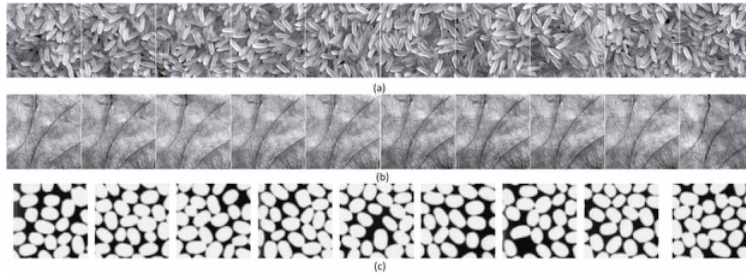
5. EXPERIMENTAL EVALUATION

To verify the effectiveness of MDSI-LCvMSP, the authors conducted a series of tests on two texture databases: Kylberg (The Kylberg Texture Dataset, 2011) and Brodatz texture database (Wang et., 2020). Considering that palmprint is also a picture with rich texture information, relevant tests are also carried out using a palmprint image database (Khalid et., 2003) provided by Hong Kong Polytechnic University. The recognition rate of the proposed MDSI-LCvMSP is compared with that of a series of related algorithms. To directly reflect the ability of texture feature extraction of each algorithm, a relatively simple nearest neighbor classification method is adopted.

5.1 Database

The Kylberg texture image database contains 28 kinds of texture images, each of which contains 160 different texture images. The size of each image is 576×576 pixels and the image format is PNG. Figure 3 (a) shows 10 images of one texture in the Kylberg texture database. In the following experiment, the authors selected 28 kinds of texture samples, and 20 pictures of each kind were selected to form the experimental picture library. The palmprint database is taken from the PolyU palmprint image database provided by Hong Kong Polytechnic University. A total of 3000 palmprint images of 300 kinds of palmprint were selected, with 10 palmprint images of each subject. In our experiments, by using a similar preprocessing approach described in the literature (Zhang et al., 2003), the central 128x128 part of each palmprint image is cropped for further processing. Fig. 3 (b) is 10 pictures of one palm. Brodatz texture image database is a widespread natural texture image database, from which 100 kinds of textures are selected, 9 pictures of each kind; 900 pictures constitute the experimental image database, and the selected pictures are transformed into gray images. Fig. 3 (c) shows 9 pictures of a Brodatz texture. All pictures were resized to 64×64.

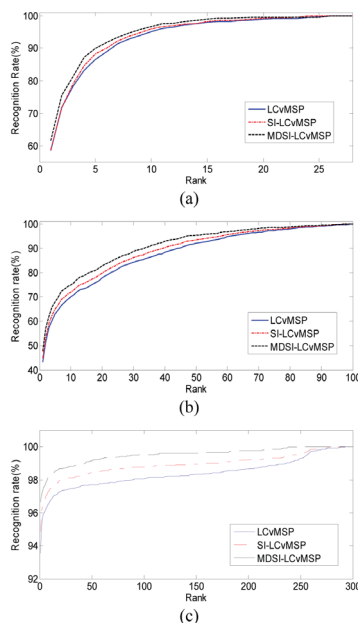
Figure 3. Preprocessed sample images (a) 10 samples of one kind of texture in Kylberg texture image database, (b) 10 samples of one kind of textures in Brodatz texture database, and (c) 10 samples of one palm in PolyU palmprint image database



5.2 Cumulative Matching Characteristic Curve

When measuring the performance of an image classification/recognition system, the index of cumulative matching curve (CMC) is often used. To calculate the cumulative matching characteristic curve of the system, it is usually necessary to build a “Gallery” library set and a “probe” library set. A Gallery set can be constructed by randomly choosing one image from each class of images in the database, and the probe set can be composed of the remaining samples after the gallery set is removed from the database. The calculation of the cumulative matching characteristic curve is introduced in detail (Ziqing(2004)). When calculating the CMC curve of the Kylberg image database, select one image from each class texture in the Kylberg image library constructed in Section 5.1 to form the “Gallery” image library, and the remaining images form the “probe” image database. When using Brodatz texture and palmprint images to calculate CMC, the authors also chose one image of each class to form the “Gallery” image library, and the rest to form the “probe” image database. The proposed MDSI-LCvMSP is compared with LCvMSP, SI-LCvMSP in CMC.

Figure 4. Cumulative matching characteristic curve of each image database (a) Kylberg image database, (b) Brodatz image database, and (c) PolyU palmprint image database of Hong Kong Polytechnic University



As can be seen from Figure 4, MDSI-LCvMSP explores shape index with more directions than classical LCvMSP and obtains a higher recognition rate than LCvMSP and SI-LCvMSP. The rank 1 recognition rates of LCvMSP, SI-LCvMSP and MDSI-LCvMSP in the Kylberg image database are 58.52%, 58.65%, and 61.47%, respectively. The rank 1 recognition rates of LCvMSP, SI-LCvMSP, and MDSI-LCvMSP in the Brodatz image database are 43.26%, 44.70%, and 47.73%, respectively. The rank 1 recognition rates of LCvMSP, SI-LCvMSP, and MDSI-LCvMSP in the palmprint database are 93.56%, 94.85%, and 96.67%, respectively. As the difference between within-class samples from Kylberg database or Brodatz database is huge, the recognition rate on two such databases are low. We can use the color information of two such databases to enhance the recognition rate. Because palmprint is a relatively stable texture image, the recognition rate in palmprint database is excellent compared with other the recognition rates in other databases.

5.3 Comparison of Correct Recognition Rate

The recognition rate of the system is an important index to measure the system performance. This section compares and analyzes the recognition rates of the proposed MDSI-LCvMSP algorithm and some related algorithms, including LCvMSP (El Merabet & Ruichek, 2018), SI-LCvMSP (Alpaslan & Hanbay, 2020), CLBP (Guo et al., 2010), and LCCP plus LBP (Xi et al., 2016). The authors randomly selected three images from each class texture image in the Brodatz image database, the Kylberg texture image database, and the PolyU palmprint database of Hong Kong Polytechnic University to construct the training image set, and the rest of each training set is the corresponding testing image set. Since the Brodatz image database contains nine pictures of each class, there are three training pictures of each class and six testing pictures of each class. The Kylberg image database contains 20 pictures of each class, three training pictures of each class, and 17 testing pictures of each class. The palmprint image database used in our experiments contains 10 images of each class, three training images of each class, and seven testing images of each class. The test is repeated for five times, the average recognition rate and standard deviation of each algorithm are calculated, and the recognition results are listed in Table 1. It can be seen from Table 1 that the average recognition rates of MDSI-LCvMSP algorithm on Kylberg, Brodatz, and palmprint databases are 62.57%, 47.27%, and 96.75% respectively, which have certain advantages compared with other algorithms. In addition, it can be seen from table 1 that SI-LCvMSP has better recognition performance than LCvMSP, which indicates that shape index is indeed a powerful tool for texture description, which is consistent with the conclusion in the literature (Alpaslan & Hanbay, 2020). In addition, the recognition performance of LCCP plus LBP algorithm also has certain advantages compared with other algorithms.

Table 1. Comparison with related algorithms (average recognition rate (%) and standard deviation)

Methods	Datasets		
	Kylberg	Brodatz	PolyU palmprint
MDSI-LCVMSP	62.57±1.8	47.27±1.9	96.75±2.0
LCvMSP (Koenderink & Van Doorn, 1992)	61.25±2.3	45.73±2.2	95.42±1.9
SI-LCvMSP (El Merabet & Ruichek, 2018)	62.73±2.1	46.85±1.9	96.54±2.1
ARCS-LBP (Chakraborty et al., 2018)	60.38±2.3	44.35±1.8	95.28±2.1
CLBP (Guo et al., 2010)	53.12±1.8	40.28±2.1	93.34±1.9
CSQP (Dubey, 2019b)	56.21±2.2	41.73±1.7	93.26±2.0
FDLBP (Ding et al., 2016)	59.65±1.8	44.18±1.9	95.35±2.3
LCCP plus LBP (Alpaslan & Hanbay, 2020)	61.13±1.7	45.27±2.0	94.48±1.9
LBDP (Dubey, 2019a)	53.56±1.8	41.63±2.2	93.45±2.1

Table 1 continued on next page

Table 1 continued

Methods	Datasets		
	Kylberg	Brodatz	PolyU palmprint
LOOP (Verma & Raman, 2017)	53.65±2.2	40.14±1.9	93.23±2.0
LBP (Ojala et al., 2002)	58.25±1.8	43.17±2.2	95.15±2.1
DRLBP (El merabet et al., 2019)	57.34±1.9	42.36±2.3	94.38±2.1
ILBP (Sucharitha & Senapati, 2019)	53.26±2.0	41.17±1.7	93.27±1.8
LDN (Jin et al., 2004)	54.74±2.2	41.25±2.1	93.56±1.9
LDRP (Rivera et al., 2013)	54.33±1.9	40.36±2.2	93.78±1.8
LDEBP (Chakraborti et al., 2018)	53.35±2.3	41.34±2.2	93.83±2.1
DCP (Dubey et al., 2016)	55.38±1.7	41.86±1.8	93.23±1.9
LNDP (Zhang et al., 2007)	54.15±2.3	40.23±1.9	93.13±2.1

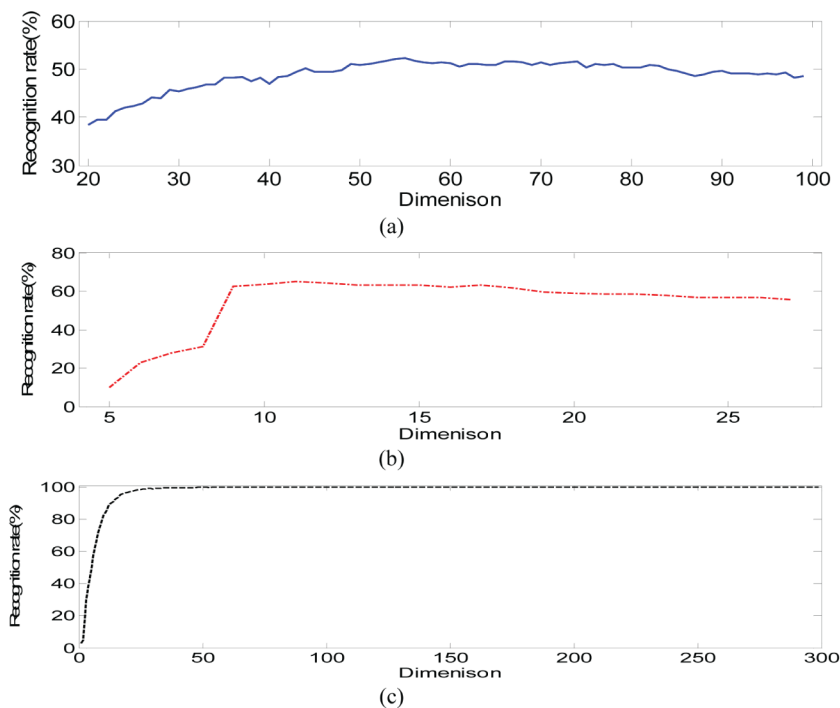
We compared the computational complexity of the first five algorithms with better performance in Table 1. The time consumed on the feature extraction of an image with MDSI-LCvMSP, LCvMSP, SI-LCvMSP, ARCS-LBP, and LCCP plus LBP are considered. Experiments were implemented on a computer system of PIV 3.3 GHz and 8 GB RAM with Matlab 2014b. The times consumed of MDSI-LCvMSP, LCvMSP, SI-LCvMSP, ARCS-LBP, and LCCP plus LBP are 0.4415s, 0.0059s, 0.0224s, 0.0013s, and 0.0106s, respectively. Because four scales and five directions are used in MDSI-LCvMSP algorithm, the time consumed by MDSI-LCvMSP algorithm is almost 20 times that of SI-LCvMSP. Of course, a delay of 0.4415s is tolerable in the actual system.

5.4 Performance Analysis of Feature Vectors Under Different Dimensions

The proposed MDSI-LCvMSP algorithm first extracts the two-order gradient features in each direction and scale of the image, then calculates the modified shape index of each gradient feature matrix, then finally calculates the LCvMSP histogram feature vector of each shape index matrix and connects each histogram feature vector to obtain the final matching feature vector. The size of the image used in the experiment is 64x64 pixels, and then the two-order gradient of the image under different scales and directions is calculated. In the experiment, four gradients and five directions are used, so 20 two-order gradient matrices can be obtained for each image, and then the modified shape index of each gradient matrix is calculated to obtain 20 modified shape index matrices. Next, each modified shape index matrix is divided into nonoverlapping 4x4 blocks and the feature vectors of the local convex and concave microstructure pattern of each subblock are calculated. In the experiment, if the length of histogram feature vector of local convex and concave microstructure pattern is set to 128, the length of the final feature vector of an image is $20 \times 4 \times 4 \times 128 = 40960$. Clearly, the final feature vector is too long, which brings more burden on save and matching of feature vectors, and too long feature vectors inevitably introduce noise. Therefore, reducing the length of feature vectors can save the storage space and reduce the computing power required for feature vector matching. Simultaneously, it should also improve the recognition rate of the feature vectors. In the experiment, principal component analysis plus linear discriminant analysis (PCA plus LDA) is used to reduce the dimension of feature vector (Martinez & Kak, 2012). In the PCA plus LDA method, PCA firstly is used to reduce the dimension of all eigenvectors to $N^T - c$, and then LDA is used to obtain the $c - 1$ eigenvectors, where N^T represents the total number of training samples and c represents the number of classes

in training samples (Martinez & Kak, 2012; Xi & Zhang, 2010; Xi et al., 2012). The feature vectors obtained from MDSI-LCvMSP are projected into the projection subspace constructed by the $c - 1$ feature vectors to obtain the dimension-reduced feature vectors. The feature vectors after dimensionality reduction are matched by Euclidean distance and classified by the nearest neighbor classifier. In the Kylberg database, Brodatz database, and the PolyU palmprint database of Hong Kong Polytechnic University, the authors randomly selected 3 pictures of each subject to construct the training set, and other pictures to construct the testing set, then used MDSI-LCvMSP to obtain the feature vector of each picture, and finally used PCA plus LDA to reduce the dimension of the feature vector to obtain the recognition rate and draw the relationship between the recognition rate and the dimension of the feature vector in Figure 5. In Figure 5, it can be seen that the highest recognition rates of the kylberg database, Brodatz database, and the PolyU palmprint database of Hong Kong Polytechnic University are 52.33%, 65.00%, and 100.00%, respectively. Compared with the results in Table 1, it can be seen that the recognition result of MDSI-LCvMSP with dimension reduction is better than that of MDSI-LCvMSP, which indicates that dimension reduction reduces the redundant information between different directions of MDSI-LCvMSP.

Figure 5. Recognition rate (%) versus the dimension of feature vectors (a) Kylberg database, (b) Brodatz database, and (c) PolyU palmprint database



6. WEIGHTED MDSI-LCVMSP

For image classification/recognition, the importance of different regions in the image is different. If the sub-area of an image has rich information, its histogram should have a large weight. Our proposed weighted MDSI-LCVMSP (Weighted MDSI-LCVMSP) is listed as follows:

1. Suppose that an image I is evenly divided into nonoverlapping L regions, which are represented as $I^{(i)}$ ($i = 0, 1, 2, \dots, L$), respectively.
2. Calculate MDSI-LCvMSP feature of the i th sub-region of image in light of formula (8). The result is assumed to be $f_{MDSI-LCvMSP}^{I^{(i)}, \theta_m, \sigma_n}$ ($i = 0, 1, 2, \dots, 15$, $\sigma_n = \sigma_0, \sigma_1, \sigma_2, \sigma_3$, $\theta_m = \theta_0, \theta_1, \theta_2, \theta_3, \theta_4$).

The weighted histogram feature vector of $f_{MDSI-LCvMSP}^{I^{(i)}, \theta_m, \sigma_n}$ can be defined as follows:

$$H_{Weighted-MDSI-LCvMSP}^{I^{(i)}}(r) = \sum_{x_c=1}^N \sum_{y_c=1}^M g \left(f_{MDSI-LCvMSP}^{I^{(i)}, \theta_m, \sigma_n}(x_c, y_c), r \right) \quad (12)$$

where:

$$g \left(f_{MDSI-LCvMSP}^{I^{(i)}, \theta_m, \sigma_n}(x_c, y_c), r \right) = \begin{cases} W(x_c, y_c), & f_{MDSI-LCvMSP}^{I^{(i)}, \theta_m, \sigma_n}(x_c, y_c) = r \\ 0, & otherwise \end{cases} \quad (13)$$

where $W(x_c, y_c)$ is the weight of image I at position (x_c, y_c) and r is the index of the histogram bin. There are two ways of designing the weight matrix W . One is to directly specify the value of the weighted matrix, which can be used for face recognition as different parts of the face play different roles in face recognition (Zhang et al., 2007). Another method is to design a weight matrix by using information entropy. The weight matrix based on the information entropy of the i th block can be

calculated by $W_i = E_i / \sum_{j=1}^t E_j$, where E_i is as follows:

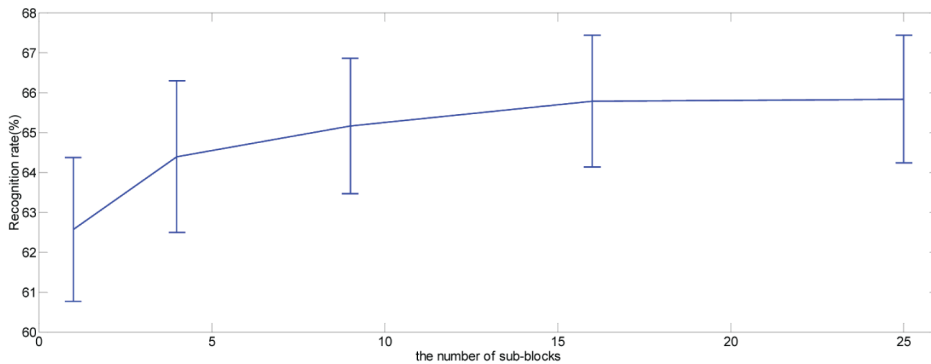
$$E_i = - \sum_{r=1}^K H_{Weighted-MDSI-LCvMSP}^{I^{(i)}}(r) \log H_{Weighted-MDSI-LCvMSP}^{I^{(i)}}(r) \quad (14)$$

K is the number of bins in the histogram vector. The weighted histogram feature vector of the i th sub-block is $W_i H_{Weighted-MDSI-LCvMSP}^{I^{(i)}}$ and the final histogram feature vector for matching is as follows:

$$H_{Weighted-MDSI-LCvMSP}^I = \left[W_1 H_{Weighted-MDSI-LCvMSP}^{I^{(1)}}, W_2 H_{Weighted-MDSI-LCvMSP}^{I^{(2)}}, \dots, W_L H_{Weighted-MDSI-LCvMSP}^{I^{(L)}} \right] \quad (15)$$

To verify the effectiveness of Weighted MDSI-LCvMSP, some experiments have been done on the Kylberg database. The authors randomly select three images from each class texture image in the Kylberg texture image database to construct the training image set, and the rest of each training set is the corresponding testing image set. Information entropy based Weighted MDSI-LCvMSP is validated and image I is divided evenly into L blocks ($L = 1, 4, 9, 16, 25$). The right recognition rate along the L is plotted in Figure 6.

Figure 6. Recognition rate (%) of Weighted MDSI-LCvMSP versus the number of sub-blocks on Kylberg database



It can be seen from Figure 6 that the recognition rates of weighted MDSI-LCvMSP algorithm on kylberg databases with the number of sub-blocks one, four, nine, 16, and 25 are 62.57%, 64.39%, 65.16%, 65.78%, and 65.83%, respectively, which have apparently enhanced the recognition rate of MDSI-LCvMSP. However, with the increase of the number of blocks, the increase of the recognition rate becomes smaller. Considering the computation complexity and recognition rate, it is better to take 16 as the number of blocks.

7. CONCLUSION

In this paper, an efficient MDSI-LCvMSP texture descriptor is proposed, which encodes the gradient information of an image in multiple directions and scales. Two extensions of MDSI-LCvMSP have also been proposed, such as Weighted MDSI-LCvMSP and projecting feature vector of MDSI-LCvMSP onto a discriminant subspace. Extensive experiments have been conducted to evaluate the performance of MDSI-LCvMSP and its extensions. Some major conclusions can be drawn:

1. MDSI-LCvMSP has a more powerful ability than SI-LCvMSP when considering multiple directions and scales of gradient, which can be seen from Figure 4, Figure 5, Figure 6 and Table 1.
2. As the size of feature vector of MDSI-LCvMSP is larger than SI-LCvMSP and there is redundant information between eigenvectors of SI-LCvMSP in different directions and scales, the eigenvectors of MDSI-LCvMSP can be projected onto a discriminant subspace to obtain shorter and more discriminative MDSI-LCvMSP feature vectors.
3. Weighted MDSI-LCvMSP with weight assignment improves the performance of MDSI-LCvMSP, which is shown in Figure 6.

Although MDSI-LCvMSP consumes more time than SI-LCvMSP, it can be improved by pre-allocating memory for Gaussian filter template, which is also the direction of the authors' next improvement. Another future direction is to explore more extensions of multidirectional shape index.

COMPETING INTERESTS

The authors of this publication declare there are no competing interests.

FUNDING AGENCY

This work was funded by the National Natural Science Foundation of China with grant number 61762022, doctoral startup fund of Guizhou Normal University 2017 with grant number 0517075, and the special project of academic new seedling cultivation and innovation exploration with grant number (2017)5726.

REFERENCES

- Alata, O., Cariou, C., Ramananjarasoa, C., & Najim, M. (1998). Classification of rotated and scaled textures using HMHV Spectrum Estimation and the Fourier-Mellin Transform. *Proc. IEEE Int'l Conf. Image Processing, 1*, 53-56. doi:10.1109/ICIP.1998.723414
- Alpaslan, N., & Hanbay, K. (2020). Multi-scale shape index-based local binary patterns for texture classification. *IEEE Signal Processing Letters, 9*, 1-5. doi:10.1109/LSP.2020.2987474
- Andrearczyk, V., & Whelan, P. F. (2016). Using filter banks in Convolutional Neural Networks for texture classification. *Pattern Recognition Letters, 84*, 63-69. doi:10.1016/j.patrec.2016.08.016
- Bovik, A. C. (1990). Multichannel texture analysis using localized spatial filters. *IEEE Transactions on Image Processing, 12*(1), 55-73.
- Bu, X., Wu, Y., Gao, Z., & Jia, Y. (2019). Deep convolutional network with locality and sparsity constraints for texture classification. *Pattern Recognition, 91*, 34-46. doi:10.1016/j.patcog.2019.02.003
- Chakraborti, T., Mccane, B., Mills, S., & Pal, U. (2018). LOOP descriptor: Local optimal-oriented pattern. *IEEE Signal Processing Letters, 25*(5), 635-639. doi:10.1109/LSP.2018.2817176
- Chakraborty, S., Singh, S. K., & Chakraborty, P. (2018). Centre symmetric quadruple pattern: A novel descriptor for facial image recognition and retrieval. *Pattern Recognition Letters, 115*, 50-58. doi:10.1016/j.patrec.2017.10.015
- Chan, C. H., Kittler, J., & Messer, K. (2007). Multi-scale local binary pattern histograms for face recognition. *International Conference on Advances in Biometrics*, (pp. 809-818). doi:10.1007/978-3-540-74549-5_85
- Chan, T. H., Jia, K., Gao, S., Lu, J., Zeng, Z., & Ma, Y. (2015). PCANet: A simple deep learning baseline for image classification. *IEEE Transactions on Image Processing, 24*(12), 5017-5032. doi:10.1109/TIP.2015.2475625 PMID:26340772
- Chellappa, R., & Chatterjee, S. (1985). Classification of textures using Gaussian Markov random fields. *IEEE Transactions on Acoustics, Speech, and Signal Processing, 33*(4), 959-963. doi:10.1109/TASSP.1985.1164641
- Chen, X., Zhang, J., & Li, D. (2012). Direct discriminant locality preserving projection with Hammerstein polynomial expansion. *IEEE Transactions on Image Processing, 21*(12), 4858-4867.
- Chen, X., Zhou, Z., Zhang, J., Liu, Z., & Huang, Q. (2016). Local convex-and-concave pattern: An effective texture descriptor. *Information Sciences, 363*, 120-139.
- Cohen, F. S., Fan, Z., & Patel, M. A. (1991). Classification of Rotated and Scaled Texture Images Using Gaussian Markov Random Field Models. *IEEE Transactions on Pattern Analysis and Machine Intelligence, 13*(2), 192-202. doi:10.1109/34.67648
- Ding, C., Choi, J., Tao, D., & Davis, L. S. (2016). Multi-directional multi-level dual-cross patterns for robust face recognition. *IEEE Transactions on Pattern Analysis and Machine Intelligence, 38*(3), 518-531. doi:10.1109/TPAMI.2015.2462338 PMID:27046495
- Dubey, S. R. (2019a). Face retrieval using frequency decoded local descriptor. *Multimedia Tools and Applications, 78*(12), 16411-16431. doi:10.1007/s11042-018-7028-8
- Dubey, S. R. (2019b). Local directional relation pattern for unconstrained and robust face retrieval. *Multimedia Tools and Applications, 78*(19), 28063-28088. doi:10.1007/s11042-019-07908-3
- Dubey, S. R., Singh, S. K., & Singh, R. K. (2016). Local bit-plane decoded pattern: A novel feature descriptor for biomedical image retrieval. *IEEE Journal of Biomedical and Health Informatics, 20*(4), 1139-1147. doi:10.1109/JBHI.2015.2437396
- Gang, L. I., Haifang, L. I., Shang, F., & Guo, H. (2018). Noise image segmentation model with adaptive neighborhood based on gradient information. *Computer Engineering, 44*(5), 233-239.
- Gatys, L. A., Ecker, A. S., & Bethge, M. (2016). Image style transfer using convolutional neural networks. In *CVPR* (pp. 2414-2423). doi:10.1109/CVPR.2016.265

- Guo, Z., Zhang, L., & Zhang, D. (2010). A completed modeling of local binary pattern operator for texture classification. *IEEE Transactions on Image Processing*, 19(6), 1657–1663. doi:10.1109/TIP.2010.2044957 PMID:20215079
- Han, J., & Ma, K. (2007). Rotation invariant and scale invariant gabor features for texture image retrieval. *Image and Vision Computing*, 25(9), 1474–1481. doi:10.1016/j.imavis.2006.12.015
- Haralick, R. M., Shanmugam, K., & Dinstein, I. H. (1973). Texture features for image classification. *IEEE Transactions on Systems, Man, and Cybernetics*, 3(6), 610–621. doi:10.1109/TSMC.1973.4309314
- Jin, H., Liu, Q., Lu, H., & Tong, X. (2004). Face detection using improved LBP under Bayesian framework. In *Proceedings of the 3rd International Conference on Image and Graphics*, (pp. 306-309).
- Julesz, B. (1962). Visual pattern discrimination. *I.R.E. Transactions on Information Theory*, 8(2), 84–92. doi:10.1109/TIT.1962.1057698
- Khalid, N., Ahmad, M. I., Mandeel, T. H., & Isa, M. (2021). Palmprint features matching based on kaze feature detection. *Journal of Physics: Conference Series*, 1878(1), 012055 (7pp).
- Koenderink, J. J., & Van Doorn, A. J. (1992). Surface shape and curvaturescales. *Image and Vision Computing*, 10(8), 557–564. doi:10.1016/0262-8856(92)90076-F
- Kylberg, G. (n.d.). The Kylberg Texture Dataset v. 1.0, Centre for Image Analysis, Swedish University of Agricultural Sciences and Uppsala University, External report (Blue series) No. 35. <https://www.cb.uu.se/~gustaf/texture/>
- Li, S., & Jain, A. (2004). Handbook of Face Recognition. 'Chapter 14: Performance Evaluation.' Springer-Verlag.
- Liao, J., Li, B., Wang, J., Qi, Q., & Li, T. (2018). Rapid relevance feedback strategy based on distributed CBIR system. *International Journal on Semantic Web and Information Systems*, 14(2), 26. doi:10.4018/IJSWIS.2018040101
- Liao, S., Law, M., & Chung, A. (2009). Dominant local binary patterns for texture classification. *IEEE Transactions on Image Processing*, 18(5), 1107–1118. doi:10.1109/TIP.2009.2015682 PMID:19342342
- Liu, J., Yuan, K., Zhou, J., & Shi, J. (2018). Study on ontology ranking models based on the ensemble learning. *International Journal on Semantic Web and Information Systems*, 14(2), 24.
- Mallat, S. G. (1989). A theory for multiresolution signal decomposition: The wavelet representation. *IEEE Transactions on Pattern Analysis and Machine Intelligence*, 11(7), 674–693. doi:10.1109/34.192463
- Manian, V., & Vasquez, R. (1998). scaled and rotated texture classification using a class of basic functions. *Pattern Recognition*, 31(12), 1937–1948. doi:10.1016/S0031-3203(98)00053-3
- Martinez, A. M., & Kak, A. C. (2012). PCA versus LDA. *IEEE Transactions on Pattern Analysis and Machine Intelligence*, 23(2), 228–233. doi:10.1109/34.908974
- Mehta, R., & Egiazarian, K. (2015). Dominant Rotated Local Binary Patterns (DRLBP) for texture classification. *Pattern Recognition Letters*, 71, 16–22. doi:10.1016/j.patrec.2015.11.019
- Merabet, Y. E., & Ruichek, Y. (2018). Local concave-and-convex microstructure patterns for texture classification. *Pattern Recognition*, 76, 303–322. doi:10.1016/j.patcog.2017.11.005
- Merabet, Y. E., Ruichek, Y., & Idrissi, A. E. (2019). Attractive-andrepulsive center-symmetric local binary patterns for texture classification. *Engineering Applications of Artificial Intelligence*, 78, 158–172. doi:10.1016/j.engappai.2018.11.011
- Ojala, T., Pietikainen, M., & Maenpaa, T. (2002). Multiresolution grayscale and rotation invariant texture classification with local binary patterns. *IEEE Transactions on Pattern Analysis and Machine Intelligence*, 24(7), 971–987. doi:10.1109/TPAMI.2002.1017623
- Oyallon, E., & Mallat, S. (2015). Deep roto-translation scattering for object classification. In CVPR, 2865-2873. doi:10.1109/CVPR.2015.7298904
- Pietikainen, M., Hadid, A., Zhao, G., & Ahonen, T. (2011). *Computer vision using local binary patterns*. Springer. doi:10.1007/978-0-85729-748-8

- Ramí, A. N., Rivera, R., Castillo, J. R., & Chae, O. O. (2013). Local directional number pattern for face analysis: Face and expression recognition. *IEEE Transaction on Image Processing*, 22(5), 1740-1752.
- Randen, T., & Husy, J. H. (1999). Filtering for texture classification: A comparative study. *IEEE Transactions on Pattern Analysis and Machine Intelligence*, 21(4), 291-310. doi:10.1109/34.761261
- Seddik, A. (2022). AI-enabled digital forgery analysis and crucial interactions monitoring in smart communities. *Technological Forecasting and Social Change*, 177, 177. doi:10.1016/j.techfore.2022.121555
- Song, Y., Zhang, S., He, B., & Sha, Q., Shen, Y., Yan, T., Nian, R., & Lendasse A. (2018). Gaussian derivative models and ensemble extreme learning machine for texture image classification. *Neurocomputing*, 277, 53-64.
- Srivastava, A. M., Rotte, P. A., Jain, A., & Prakash, S. (2022). Handling data scarcity through data augmentation in training of deep neural networks for 3D data processing. *International Journal on Semantic Web and Information Systems*, 18(1), 16. doi:10.4018/IJSWIS.297038
- Sucharitha, G., & Senapati, R. K. (2019). Biomedical image retrieval by using local directional edge binary patterns and Zernike moments. *Multimedia Tools and Applications*, 79, 1-18.
- Thanh, L. T. V. (2022). A Model of Semantic-Based Image Retrieval Using C-Tree and Neighbor Graph. In *World Conference on Information Systems and Technologies*. Springer, Cham. doi:10.1007/978-3-031-04819-7_18
- Varma, M., & Garg, R. (2007). Locally invariant fractal features for statistical texture classification. In *Proc. International Conference on Computing Vision* (pp. 1-8).
- Verma, M., & Raman, B. (2017). Local neighborhood difference pattern: A new feature descriptor for natural and texture image retrieval. *Multimedia Tools and Applications*, 77, 1-24.
- Vu, N. S. (2003). Exploring patterns of gradient orientations and magnitudes for face recognition. *IEEE Transactions on Information Forensics and Security*, 8(2), 295-304.
- Wang, H., Qu, H., Xu, J., Wang, J., & Zhang, Z. (2020). Combining statistical features and local pattern features for texture image retrieval. *IEEE Access: Practical Innovations, Open Solutions*, 8, 222611-222624. doi:10.1109/ACCESS.2020.3043413
- Wu, Y., & Yoshida, Y. (1995). An efficient method for rotation and scaling invariant texture classification. *Proceedings of the IEEE International Conference on Acoustics, Speech, and Signal Processing*, 4, 2519-2522.
- Xi, C., & Zhang, J. (2010). Maximum variance difference based embedding approach for facial feature extraction. *International Journal of Pattern Recognition and Artificial Intelligence*, 24(7), 1047-1060.
- Xi, C., & Zhang, J. (2011). Illumination robust single sample face recognition using multi-directional orthogonal gradient phase faces. *Neurocomputing*, 74(14), 2291-2298.
- Xi, C., & Zhang, J. (2014). Biometric feature extraction using local fractal auto-correlation. *Chinese Physics B*, 23(9), 96401-1-096401-6.
- Zhang, B., Gao, Y., Zhao, S., & Liu, J. (2010). Local derivative pattern versus local binary pattern: Face recognition with higher-order local pattern descriptor. *IEEE Transactions on Image Processing*, 19(2), 533-544.
- Zhang, B., Shan, S., Chen, X., & Gao, W. (2007). Histogram of Gabor Phase Patterns (HGPP): A novel object representation approach for face recognition. *IEEE Transactions on Image Processing*, 16(1), 57-68.
- Zhang, D. D., Kong, W., You, J., & Wong, M. (2003). Online palmprint identification. *IEEE Transactions on Pattern Analysis and Machine Intelligence*, 25(9), 1041-1050.
- Zhang, T., Yuan, Y. T., Fang, B., Shang, Z., & Liu, X. (2009). Face recognition under varying illumination using gradientfaces. *IEEE Transactions on Image Processing*, 18(11), 2599-2606.
- Zhang, J., Marszałek, M., Lazebnik, S., & Schmid, C. (2007). Local features and kernels for classification of texture and object categories: A comprehensive study. *IJCV*, 73(2), 213-238.
- Zhao, G., & Pietikainen, M. (2007). Dynamic texture recognition using local binary patterns with an application to facial expressions. *IEEE Transactions on Pattern Analysis and Machine Intelligence*, 29(6), 915-928.

Zheng, L., Yang, Y., & Tian, Q. (2018). SIFT meets CNN: A decade survey of instance retrieval. *IEEE Transactions on Pattern Analysis and Machine Intelligence*, 40(5), 1224–1244.

Xi Chen received his doctorate in pattern recognition and biometrics from Sichuan province key laboratory of signal and information processing, Southwest Jiao Tong University, Chengdu, China in 2011. He joined Kunming University of Science and Technology in 2011. He joined Guizhou Normal University in 2016. His current research interests include digital signal processing, pattern recognition, and biometrics.

Jiangmei Li graduated from Kai Li University with a bachelor's degree in computer network engineering. She is currently a master's student of Guizhou Normal University. Her current interests include image processing and pattern recognition.

Yun Fei Zhang graduated from North China University of water resources and hydropower with a bachelor's degree in computer network engineering. He is currently a master's student of Guizhou Normal University. His current interests include image processing and pattern recognition.